Optimal FBG Sensor Deployment via Gaussian Quadrature Formula for Measurement of Displacement of Laterally Loaded Piles

Le déploiement optimal des capteurs à fibres optiques, par la formule de la quadrature de Gauss, pour la mesure du déplacement des pieux chargés latéralement

Jung Y.-H., Na S.-U., Mok Y.
Dept. of Civil Engineering, Kyung Hee University, Republic of Korea

ABSTRACT: A new approach to sensor deployment for measurement of lateral displacement of piles is introduced. To monitor a pile loaded by lateral loads, the multiplexed Fiber-optic Bragg Grating (FBG) sensors are used. For enhanced accuracy of measurement under budgetary limitation, optimal position of the FBG sensors inscribed along an intact optic fiber line is crucial. Herein, ideal test conditions under which test results could be verified through theoretical solutions were created. The integration points of the Gaussian quadrature formula were employed to determine the optimal positions to place sensors. By using differential equations on pile displacement subjected to lateral load, the measured and calculated displacements were compared. The comparative analysis shows that positioning sensors based on theoretical Gaussian quadrature formula reduces measurement errors. To minimize the errors in estimating lateral displacement under general in-situ conditions, a suggestion for the FBG sensor deployment has been given.

RESUME : Une nouvelle approche de déploiement des capteurs à fibres optiques pour la mesure du déplacement latéral des pieux est présentée. Pour surveiller un pieu chargé latéralement, les capteurs multiplexeurs à fibres optiques avec réseau de Bragg (Fiber-Optic Bragg Grating : FBG) sont utilisés. L'emplacement optimal des capteurs FBG inscrits le long d'une ligne intacte de fibre optique est crucial afin d'assurer une bonne précision de mesure, à un coût optimisé. Les conditions idéales d'essai dans lesquelles les résultats peuvent être vérifiés par des solutions théoriques ont été créées. Les points d'intégration de la formule de la quadrature de Gauss ont été utilisés pour déterminer les meilleurs emplacements des capteurs. En utilisant les équations différentielles des déplacements d'un pieu soumis à une charge latérale, les résultats des mesures et du calcul ont été comparés. L'analyse comparative montre que l'approche du déploiement des capteurs sur la base théorique de la formule de la quadrature de Gauss fonctionne très bien. Une suggestion du déploiement des capteurs FBG est donnée afin de minimiser les erreurs d'estimation du déplacement latéral sous les conditions générales *in situ.*

KEYWORDS: Gaussian quadrature, Sensor placement, Lateral-loaded Pile, Measurements

1 INTRODUCTION

FBG sensors have been widely applied to structural monitoring because optical sensors can overcome many limitations of existing electric sensors such as electronic interference and low durability. In addition, there is an advantage that it is possible for one strand of optical fiber to be inscribed with many sensors and used as a multi-point sensor. In regard to monitoring super-structures such as railroad bridges that are frequently exposed to electromagnetic waves, the FBG sensor is successfully used for the long-term maintenance system (Chung et al. 2005).

To measure the performance of geotechnical structures such as piles, FBG sensors are superior to other electric sensors because typically the measurement for geotechnical structures should be performed in adverse environments such as high confinement, strong chemical corrosion, and narrow space. Recently, there were several attempts to measure the performance of piles. Lee, et al. (2004) have attached FBG sensors to cast-in-place concrete piles and measured the vertical load transfer process, thus presenting the usability of FBG sensors in geotechnical structures. Habel and Krebber (2011) have used fiber-optic acoustic emission sensors to measure AE signals related to the shock waves of concrete pile heads, thus evaluating the soundness of concrete piles. However, few are cases that have systematically analyzed and verified the use of FBG sensors in geotechnical structures.

Compared to the conventional point-located sensors, FBG sensors multiplexed on a single strand of fiber has a great advantage in its small occupancy of space for attachment and installation. Despite such advantages, the use of FBG sensors has not prevailed because inscribing one FBG grating on an optic fiber is still more expensive than buying a conventional strain gage sensor. Therefore, minimizing the number of sensors and optimizing sensor positions are the most urgent issue for successful deployment of FBG sensors in the industry.

Sensors can generally be placed in an area of interest either deterministically or randomly. The choice of the deployment scheme depends highly on the type of sensors, application and the environment that the sensors will operate in. Without any preferance of interest, sensors would be placed uniformly along the pile, whereas those simple schemes do not consider any cost effectiveness or optimazation to reduce measurement errors.

In this study, a new deployment scheme for multiplexed FBG sensors on the single optical fiber strand is introduced. The Gaussian quadrature formula has been employed to minimize the error in measuring the displacement of a laterally loaded pile. A model cantilever beam is used to simulate the pile. The applicability of the Gaussian quadrature formula for optimizing sensor positions has been confirmed by comparing applied and computed displacements. Three different strategies for placing sensors along the aluminum bar which represents a laterally loaded pile are developed, and accordingly eight different schemes of the sensor placement are configured. One end of the bar specimen is clamped, and the other is displaced by using the calipers. The maximum displacement is calculated by integrating the slopes and moments at the FBG sensor positions, and compared with the actual magnitude of applied displacement to suggest its geotechnical applicability.

2 THEORETICAL BACKGROUND

1.1 *Fiber-optic Bragg Grating (FBG) sensors*

FBG sensors inscribe stripe-like grating on the photosensitive fiber optic core by exposing the latter to ultraviolet (UV) radiation by periodically distributing the strength of the light. Once formed, FBG sensors serve as reflectors that reflect light with a pattern-specific wavelength. This reflected wavelength is called the Bragg wavelength and is as in Equation (1). In other words, when broad-spectrum light beams are transmitted to the FBG, light with the Bragg wavelength is reflected and remaining light with other wavelengths passes through.

$$\lambda_b = 2n_e\Lambda \tag{1}$$

where λ_b is Bragg wavelength, n_e is the effective refractive index of the fiber-optic core, and Λ is the interval of the grating inscribed on the fiber-optic core.

Changes in strain and the temperature affect the effective refractive index, n_e, and the grating period, Λ, so that the Bragg wavelength comes to shift. In comparison with the initial Bragg wavelength, λ_0, the shifted amount of wavelength, $\Delta\lambda$, is given as

$$\Delta\lambda/\lambda_0 = (1 - p_e)\varepsilon + (\alpha_f + \xi_f)\Delta T \tag{2}$$

where the first term of Eq. (2) is the amount shifted due to strain, p_e is the photoelatic constant, and ε is the strain underwent by the grating. The second term of Eq. (2) shows the shift of the wavelength caused by the change of temperature, α_f is the thermal expansion coefficient of the fiber optic, and ξ_f is the thermo-optic coefficient of the fiber optic. Because the experiments in the present study were conducted in a controlled laboratory environment, changes in the temperatures of the sensors themselves and their surroundings were negligible such that $\Delta T = 0$. Consequently, the second terms was eliminated so that it is possible easily to calculate strain from the wavelength shift as shown in Eq. (3).

$$\varepsilon = \frac{1}{1-p_e}\frac{\Delta\lambda}{\lambda_0} \tag{3}$$

where the photoelastic constant, p_e = 0.229, provided by the manufacturer.

1.2 *Integration by Gaussian quadrature*

In numerical analysis, a quadrature rule is an approximation of the definite integral of a function, usually stated as a weighted sum of function values at specified points within the domain of integration. An n-point Gaussian quadrature rule is a quadrature rule constructed to yield an exact result for polynomials of degree $2n - 1$ or less by a suitable choice of the points x_i and weights w_i for i = 1, …, n. The domain of integration for such a rule is conventionally taken as [-1, 1], so the rule is stated as

$$\int_{-1}^{1} f(x)dx \approx \sum_{i=1}^{n} w_i f(x_i). \tag{4}$$

Gaussian quadrature as above will only produce accurate results if the function *f(x)* is well approximated by a polynomial function within the range between -1.0 and +1.0. If the integrated function can be written as $f(x) = W(x)g(x)$, where $g(x)$ is approximately polynomial, and $W(x)$ is known, then there are alternative weight w'_i such that

$$\int_{-1}^{1} f(x)dx = \int_{-1}^{1} W(x)g(x)dx \approx \sum_{i=1}^{n} w'_i g(x_i). \tag{5}$$

For the simplest integration problem, i.e. with $W(x) = 1$, the associated polynomials are Legendre polynomials, $P_n(x)$, and the method is usually known as Gauss-Legendre quadrature. With the nth polynomial normalized to give $P_n(1) = 1$, the i-th Gauss node, x_i, is the i-th root of P_n. Its weight is given by (Abramowitz and Stegun 1972)

$$w_i = \frac{2}{(1-x_i^2)[P'_n(x_i)]^2} \tag{6}$$

A few order rules for solving the integration problem are listed in Table 1.

Table 1. Position of Gauss points and corresponding weights.

Number of Gaussian points, n_{gp}	Location, ξ_i	Weight, w_i
1	0.0	2.0
2	±0.57732502692	1.0
3	±0.7745966692 0.0	0.555 555 5556 0.888 888 8889

An integral having arbitrary limits can be transformed so that its limits are from -1 to +1. With $f = f(x)$, and with the substitution $x = \frac{1}{2}(1 - \xi)x_1 + \frac{1}{2}(1 + \xi)x_2$,

$$\int_{x_1}^{x_2} f(x)dx = \int_{-1}^{1} \phi d\xi \approx \sum_{i=1}^{n} w'_i \phi(\xi_i). \tag{7}$$

Thus the integrand is changed from $f = f(x)$ to $\phi = \phi(\xi)$, where ϕ incorporates the Jacobian of the transformation, $J = dx/d\xi = (1/2)(x_2 - x_1)$. If the function $\phi = \phi(\xi)$ is not a polynomial, Gauss quadrature is inexact, but becomes more accurate as more points are used.

1.3 *The differential equations of the deflection for a cantilever beam subjected to a point load*

As shown in Figure 1, lateral displacement, y, which is produced when pile heads are subjected to a lateral load, P, and not to axial load, is expressed in terms of differential equation, as in Equation (8).

$$EI\frac{d^2y}{dx^2} = M = P(l - x) \tag{8}$$

where *E* is the Young's modulus of the pile material, *I* is the moment of inertia of the section area of the pile, *x* is the distance from the pile end, and *M* is the sectional moment. Integrating Eq. (8) yields the function of the slope, *S*, as

$$S = \frac{dy}{dx} = \int_0^x \frac{d^2y}{dx^2}dx = \frac{1}{EI}(Plx - \frac{Px^2}{2}) \tag{9}$$

For the cantilever beam, the slope, $S = dy/dx$, remains zero at the clamped end (i.e., x = 0). Integrating Equation (9) again yields an expression of the lateral displacement, *y*, as

$$y = \int_0^x \frac{dy}{dx}dx = \frac{1}{EI}\left(\frac{Plx^2}{2} - \frac{Px^3}{6}\right) = \frac{Px^2}{6EI}(3l - x) \tag{10}$$

As a result, the maximum deflection, y_{max}, occurs at the point of the lateral load, given as

$$y_{max} = \frac{Pl^3}{3EI} \tag{11}$$

Note that two sequential integrations are necessary to obtain the displacement function of Eq. (10) from the moment function of Eq. (8).

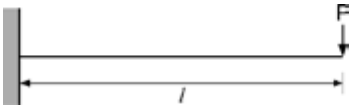

Figure 1. A cantilever beam with a concentrated load, simulating the pile subjected to a lateral load.

2 EXPERIMENTAL SETUP

2.1 *Experimental procedure*

A model cantilever beam is the aluminum bar specimen which has a physical properties listed in Table 1. Figure 1 shows the loading system including a clamp to fix one end of the bar and a calipers used to apply the displacement on the other end of the bar. In the middle points, two dial indicators were attached to measure the deflections of the bar during loading. Because the displacement is applied by using the calipers, the concentrated load, P, can be estimated as $P = (3EIy_{max})/l^3$. An optic fiber including FBG sensors inscribed at given positions was epoxied on the top surface of the bar specimen developing tensile strains during loading. Electric strain gages were glued together to validate the performance of the FBG sensors.

Figure 3. A model cantilever beam system.

Table 2. Properties of aluminum bar speciment

Length, *l* (mm)	255
Thickness, *h* (mm)	6
Width (mm)	25
Young's Modulus, *E* (Gpa)	70.56
Moment of inertial, *I* (mm^4)	450
Bending stiffness, *EI* (N·mm^2)	31,752,000

As in Eq. (11), the lateral displacement, y, is obtained by integrating Eq. (10) which is a polynomial equation with degree 2 so that two Gaussian points, ξ_1 = -0.577 and ξ_2 = +0.577, are possibly chosen according to Table 1. As shown in Figure 4, sensors were located at two points projected from two Gaussian points. The FBG sensors measure the strains via Eq. (3). When the point load, P, is applied, the cantilever beam specimen is deflected. The curvature, 1/ρ, at a section can be calculated by the strains developed on upper and lower surfaces as

$$\frac{1}{\rho} = \frac{M}{EI} = \frac{\varepsilon_e - \varepsilon_c}{h} \tag{12}$$

where ε_e is the tensile strain on upper surface, ε_c is the compressive strain on lower surface of the bar, and h is the thickness of the section of the bar specimen. Assuming that both tensile and compressive strains have the same magnitude, the sensors were attached only on the upper surface of the bar specimen. Consequently, the moment at the sections where the sensors were placed can be measured as $M = 2\varepsilon_e EI/h$.

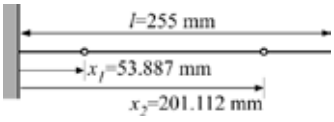

Figure 4. Optimal sensor positions for a cantilever beam

For a given displacement, theoretical values of the moment can also be computed via Eq. (9) and (11), thus $M = 3EIy_{max}(l - x)/l^3$ for a given y_{max} value. As shown in Table 3, errors in the measured moment to computed moment range between 0.15 and 1.54%, and average out to 0.82%.

Table 3. Measured and computed moments at two Gaussian points

Applied deflection, y_{max}	Moment, N-mm		
	Sensor position	x_1	x_2
1 mm	Measured	1153.6	295.3
	Computed	1155.3	309.6
	Error, %	0.15	0.46
2 mm	Measured	2290.4	612.8
	Computed	2310.7	619.2
	Error, %	0.88	1.03
3 mm	Measured	3435.6	914.458
	Computed	3465.9	928.8
	Error, %	0.88	1.54

2.2 *Optimizing sensor positions using Gaussian points*

Primary objective for deployment in this study is to minimize the error in measuring the maximum deflection at the point of loading, y_{max} . Herein, we developed three optimization strategies. The first strategy is positioning sensors at regular intervals, which is a simplest way to deploy. The second is positioning sensors at projected Gaussian points but not following the Gaussian quadrature rule. The third is positioning sensors exactly based on the Gaussian quadrature rule.

Figure 5 illustrates different deployment schemes according to first and second strategies. Four possible schemes at regular intervals are illustrated in figures on the left-hand-side column of Fig. 5, where n is the number of sensors used for each scheme. Figures on the right-hand-side column of Fig. 5 illustrate three deployment schemes using the projected Gaussian points for the number of Gaussian points, n_{gp} = 1, 2, and 3. For each case, the FBG sensors on a single strand were inscribed at positions marked as open symbols in Fig. 5. After applying y_{max} by the calipers, the strain at each sensor position was measured by FBG sensors. Subsequently two unknowns such as *P* and *l* in Eq. (8) were determined by using measured strains incorporated with the boundary condition at the clamped end, and then y_{max} was calculated via Eq. (11).

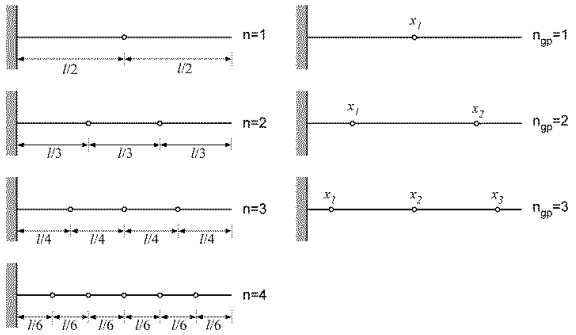

Figure 5. Different sensor deployments at regular and Gaussian points

The third strategy requires a double integral to calculate y_{max} using the moment values as described in section 2.3. Using the Gaussian quadrature rule, y_{max} can be obtained by integrating the slope function, S, which is the polynomials of degree 2, as

$$y_{max} = \int_0^l S(x)dx = \frac{l}{2}[w_1 S(x_1) + w_2 S(x_2)] \tag{13}$$

where w_1 and w_2 are weights for two Gaussian points given in Table 1, and x_1 and x_2 are the distances from the clamped end to projected Gaussian points as illustrated in Fig. 4. Because the

moment function, $M(x)$, is a first order polynomial, Eq. (13) is solved by second integral with a single Gaussian point as

$$S(x_i) = \int_0^{x_i} \frac{M(x)}{EI} dx = \frac{x_i}{2} w' \frac{M(z_i)}{EI} \quad (13)$$

where $x_i = x_1$ or x_2 in Eq. (13), w' is the weight for the single Gaussian point (i.e., $w' = 2.0$, referring to Table 1), and z_i is the sensor position projected from the Gaussian point in the range between 0 to x_i. Note that z_i is in the middle of the target length according to Table 1. Figure 6 shows the exact locations of z_i in the testing configuration.

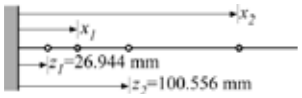

Figure 6. Optimal location of the sensors for cantilever beam

According to the different configurations for three different strategies illustrated in Figures 5 and 6, the FBG sensors were inscribed on the optic fiber attached to the bar specimen, and then the displacement was applied repeatedly by more than ten times. Table 4 compares applied and calculated values of y_{max} for the configurations with sensors positioned at the regular intervals. As the number of sensor increases, the error significantly decreases. Figure 7 shows the variation of errors against increasing applied deflection. When employing one or two sensors, the error increases as the applied deflection increases. When three or five sensors are used, the errors remain approximately constant irrespective of applied displacement.

Table 5 compares the applied and calculated values of y_{max} for the configurations with sensors positioned at the projected Gaussian points. Even in this case, the errors are also decreasing as the number of the sensors increases. For the same number of sensors, however, the error in the configuration according to the second strategy is smaller than that for the first strategy. This implies that positioning sensors deployed via the analytical formula exhibits better performance than uniformly distributed sensors.

As shown in Table 5, the error of sensors deployed with the third strategy yields much better performance than others. The average error for the third strategy is smaller by 0.2% than the error for the first strategy, and even smaller than the error for the second strategy by 0.03%. It is obvious that measuring displacement rigorously based on the Gaussian quadrature rule is superior to other cases because of its simple calculation, whereas the results indicates that increasing the number of sensors uniformly would give better measurement than employing the Gaussian quadrature rule.

Table 4. y_{max}, using sensors positioned at the regular intervals

Applied y_{max}, mm	y_{max} using 1st strategy			
	n=1	n=2	n=3	n=5
1	0.999	0.996	0.996	1.016
2	1.985	1.983	1.986	2.002
3	2.958	2.959	2.986	2.999
4	3.931	3.934	3.979	3.999
5	4.903	4.899	4.963	4.988
Average error, %	1.18	1.25	0.54	0.28

Table 5. y_{max}, using sensors positioned at projected Gaussian points

Applied y_{max}, mm	y_{max} using 2nd strategy			Using 3rd strategy
	n_{gp}=1	n_{gp}=2	n_{gp}=3	n_{gp}=2
1	0.999	0.996	0.991	1.000
2	1.985	1.982	1.995	1.982
3	2.958	2.972	2.976	2.967
4	3.931	6.949	3.943	3.941
5	4.903	4.917	4.958	4.921
Average error, %	1.18	1.04	0.84	1.01

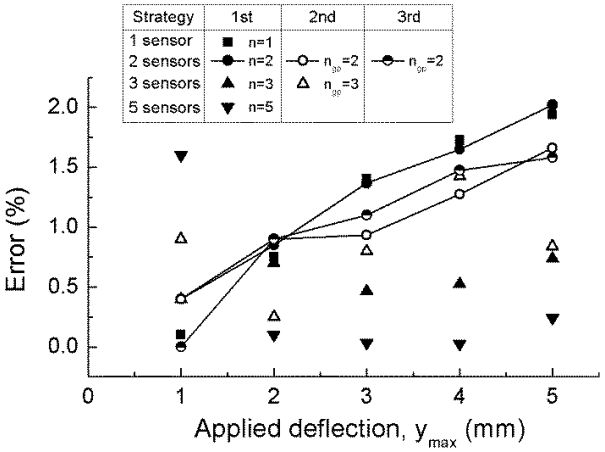

Figure 7. Errors in measurement using three different strategies

3 CONCLUSION

Using multiplexed FBG sensors require a careful deployment scheme to minimize errors in measuring lateral displacement of the pile through the least number of sensors. Herein, a new approach to deploy the FBG sensors for measurement of lateral displacement of piles was introduced. The Gaussian quadrature formula was adopted to minimize the error in measuring the deflection of a laterally loaded pile. The performance of Gaussian quadrature formula for optimizing sensor positions has been tested using the aluminum bar specimen representing a lab-scale cantilever beam with the clamped end. Primary objective for sensor deployment was set to minimize the error in measuring the maximum deflection at the point of loading. Three optimization strategies—positioning sensors at regular intervals, positioning sensors at projected Gaussian points but not following the Gaussian rule, and positioning sensors exactly based on the Gaussian rule—were implemented. In both cases for the first and second strategies, the measurement error decreases as the number of sensors increases. For the same number of sensors, however, the second strategy where the sensors were positioned at the projected Gaussian points reduces the errors by 0.2% than those for the first strategy. Positioning the sensors rigorously based on the Gaussian quadrature rule enhances the accuracy more than just using the Gaussian points. The experimental results suggested that the analytical deployment plan using the Gaussian quadrature rule can be helpful in crafting a placement in measuring the displacement of the laterally loaded pile accurately.

4 ACKNOWLEDGEMENTS

This work was supported by the National Research Foundation of Korea (NRF) grant funded by the Korean government (MEST) (No. 2009-0090774)

5 REFERENCE

Abramowitz, M. and Stegun, I.A. (1972), Handbook of Mathematical Functions, Dover, ISBN 978-0-486-61272-0

Chung, W., Kang, D.H., Choi, E.S., Kim, H.M. (2005), "Monitoring of a steel plate girder railroad bridge with fiber bragg grating sensors," Journal of Korean Society of Steel Construction, Vol. 17, No. 6, pp. 681-688.

Habel, W.R. and Krebber, K. (2011), "Fiber-optic sensor applications in civil and geotechnical engineering," Photonic sensors, Vol. 1, No. 3, pp. 268-280.

Lee, W., Lee, W.-J., Lee, S.-B., and Salgado (2004), "Measurement of pile load transfer using the Fiber Bragg Grating sensor system," Canadian Geotechnical Journal, Vol. 41, No. 6, pp. 1222-1232.